Lab on a Chip

PAPER

View Article Online
View Journal

Cite this: DOI: 10.1039/d5lc00333d

Orbital shaker-driven gut-on-a-chip platform for drug-induced permeability and microenvironment studies

Nishanth Venugopal Menon,†[ab] Jeeyeon Lee,†[cd] Hung Dong Truong,[e] Sriram Bharathkumar[e] and Chwee Teck Lim *[abce]

Gut-on-a-chip platforms replicate realistic gut microenvironments but face limited adoption due to their complex designs, expensive fabrication, and specialized instrumentation that increases operational complexity. In this study, we present a microfluidic chip insertable into 12-well plates with a unique radial design and a pumpless flow actuation system using an orbital shaker. We use a surface tension-driven hydrogel patterning technique to compartmentalize the chip, enabling co-culture of gut epithelium and vasculature, resulting in leak-proof monolayer tubes. Furthermore, computational fluid dynamic analysis demonstrates bidirectional peristaltic flow induced by the shaker. The platform's physiological relevance is confirmed through the evaluation of cell polarization, tight junction markers and barrier integrity, using high-magnification microscopy and electrical resistance measurements. We also demonstrate the ability of the platform to support live bacterial colonization, simulating host–microbe interactions. The model is validated for drug development by assessing gut and vascular permeability following drug overdose and inflammatory cytokine activation. Additionally, we explore nanoplastic poisoning using nano polyethylene terephthalate (PET) particles, highlighting the gut's role in limiting particle absorption into the bloodstream. The orbital gut-on-a-chip platform offers an accessible, dynamic cell culture system for drug discovery and biomimetic modeling of gut-related disease interactions.

Received 8th April 2025,
Accepted 31st July 2025

DOI: 10.1039/d5lc00333d

rsc.li/loc

Introduction

Gaps in preclinical testing have led to an increasing interest in organ-on-a-chip technology for drug discovery and disease modeling.[1,2] Conventional *in vitro* assays, such as static cell culture platforms[3] and Transwell inserts,[4] are limited by their simplicity and lack of control over biochemical and biomechanical cues, which affects their physiological relevance. Alternatively, 3D organoids show promise to replicate the *in vivo* cellular complexity. However, these low-throughput models do not capture the physiologically relevant biomechanical cues.[5] The discrepancies between animal models and humans further underscore the need for alternative biological models.[6,7] Organ-on-a-chip models offer dynamic physiological conditions, including shear stress,[8] motility,[9,10] oxygen gradients,[11] and 3D geometries,[12,13] to recreate the *in vivo* microenvironment. Their miniature design and potential for incorporating various analysis modalities make them valuable for preclinical studies. However, their adoption has been hindered by specialized operational requirements, such as complex instrumentation for dynamic cultures, and intricate chip design and assembly. One example is the use of fluid-actuating syringe or pressure pumps to drive organs-on-chips, which increases the footprint, cost, and handling challenges.[14,15]

Pumpless organs-on-chips show promise in addressing the footprint and handling challenges associated with operational complexity. Passive approaches including gravity-driven[16–18] and capillary-driven[19,20] flow have been useful in recreating intact organ microenvironments. Active methods involving centrifugation[21] and rocker systems[22–24] also hold potential but have limitations. For instance, passive systems suffer from inconsistent flow profiles and chip-to-chip variability, while centrifugation does not support long-term culture, and the rocker method is unsuitable for host–microbe studies. Of all these methods, only the rocker-based approach supports high-throughput operation. Besides chip operation, existing organ-on-a-chip models suffer from unharmonized designs and assembly. Low-cost organs-on-

[a] *Mechanobiology Institute, National University of Singapore, Singapore, 117411 Singapore. E-mail: ctlim@nus.edu.sg*
[b] *Institute for Digital Molecular Analytics and Science, Nanyang Technological University, 636921, Singapore*
[c] *Institute for Health Innovation and Technology (iHealthtech), National University of Singapore, Singapore, 117599 Singapore*
[d] *Biomedical Engineering Programme, City University of Hong Kong (Dongguan), Dongguan, 523808, China*
[e] *Department of Biomedical Engineering, National University of Singapore, 117583, Singapore*
† These authors contributed equally to this work.

chips using adhesives[15] and inventive connector networks[25] have been developed to reduce fabrication costs and ease operational challenges. While the former does not favor dynamic cell culture, the latter approach requires unique connectors, exacerbating the challenges associated with unharmonized designs.

Gut-on-a-chip[1] is a class of organ-chips that recapitulate the functioning of the human intestine. Previously, gut chips from single-layer designs[8,26] to multi-layered assemblies have been demonstrated,[9,24,27] each focusing on unique aspects of gastrointestinal disease. While microfabrication favors easy design modification and sophisticated geometries, the lack of standard design features and challenges in chip assembly hinder widespread use. Trietsch *et al.*[28] demonstrated a single-layered gut-on-a-chip pre-designed into a standard 384-well plate to house 40 to 64 microfluidic chips, unlike the multi-layered chips which are operated singularly or in a low-throughput configuration. However, this parallelized setup demands specialized instrumentation for pumpless operation and limits user flexibility. We realized a need for a novel design for easy assembly and a facile approach for recreating a mechanistic gut model for the heterogeneous physiology of the human gut that comprises a microbiota-enriched gut epithelium and endothelium.

Inspired by cell culture inserts, we designed a radial gut-on-a-chip that fit within the wells of a standard 12-well plate. To recreate a mechanically active gut microenvironment and simplify operability, we used standard orbital shakers to simulate fluid flow and culture gut epithelium with bacteria, and endothelial cells. The radial design ensures fluid flow through the channels from the planar rotation of the orbital shaker. We compartmentalized the chip using a previously reported extracellular matrix (ECM) patterning[29,30] method to co-culture multiple cell types. Using this approach, the chip is partitioned into three with the ECM (collagen type I) gel filling the center and two cell culture channels on either side. Gut epithelial cells (Caco-2) and vascular cells (human umbilical vein endothelial cells (HUVECs)) are cultured in the inner and outer channels, respectively, forming monolayer tubes along the channel walls. Gut bacteria can be cultured in the inner channel within the intact gut tube. Computational fluid dynamics (CFD) was employed to profile shear stress and velocity inside the cell culture channels and molecule diffusion within the collagen gel due to orbital rotation. The shaker creates a bidirectional peristaltic flow between the inlet and the outlet of the channels. We characterized the leakiness of epithelial and endothelial tubes using dextran permeability assays, measured their barrier integrity *via* transepithelial electrical resistance (TEER) and visualized gut epithelial markers such as ezrin and zonula occludens-1 (ZO-1) and endothelial cell junction markers (VE-cadherin). The platform effectively recapitulated known responses to drug overdosage and vascular inflammation, confirming its effectiveness in modeling a biomimetic gut-vasculature model. Additionally, it demonstrated the ability to study nanoplastic infiltration from the gut to blood vessels, supporting the *in vivo* route for micro-/nanoplastics entering the human bloodstream. Taken together, our studies highlight the ability to create an effective gut-on-a-chip platform using a standard orbital shaker for pertinent permeability studies crucial in drug toxicity assessment and modeling conditions like leaky gut and nanoparticle infiltration into the vasculature. This membraneless and pumpless platform is user-friendly and easy to produce, enabling its adoption without specialized personnel or instrumentation.

Results

ECM-patterned radial microfluidic chip

The microfluidic chip is a polydimethylsiloxane (PDMS)-based device with a unique radial design that allows its insertion into a standard 12-well plate. Importantly, the chip comprises 3 interconnected channels: a shallow center channel (height = 160 μm), and deeper side channels (height = 200 μm). Extracellular matrix patterning is achieved from this height difference that creates a capillary burst valve (CBV) facilitating liquid pinning to the central channel without leaking to the adjacent channels.[29] We use collagen type I as the ECM and confine it into the shallow channel, compartmentalizing the chip into three distinct channels: the central channel with ECM and two adjacent channels (Fig. S1). The side channels have a rectangular cross section, with collagen gel forming one side and PDMS comprising the other three sides of the channel (Fig. 1A). Gut epithelium and endothelium were cultured along the walls, including the exposed surface of the collagen gel. The PDMS chips were bonded to circular glass coverslips (Φ = 21 mm) for easy insertion into the wells of a 12-well plate (well Φ = 22 mm) (Fig. 1B). An additional layer of PDMS was bonded to the PDMS to house the reservoirs for cell culture media. To stimulate fluid flow through the channels, the chips were placed on an orbital shaker operated at 100 rpm (Fig. 1C). The planar surface of the orbital shaker ensures that every point on the surface of the shaker experiences the same forces. A standard orbital shaker with a surface of ~30 mm × 30 mm can accommodate four 12-well plates with the option of stacking multiple well plates on top of each other. This facilitates a high-throughput operation of 100 to 200 chips simultaneously. Gut epithelial cells (Caco-2) and endothelial cells (HUVECs) were cultured in the inner and outer channels, respectively (Fig. 1D). The cells formed confluent monolayer tubes within 4 days of culture under normoxic conditions of 5% CO_2 and 37 °C and 100 rpm orbital shaking. The platform replicates a section of intestinal villi, with a monolayer of gut epithelial cells and vascular cells separated by a basement membrane. In addition to enabling high-throughput cultures, the use of glass coverslips facilitates integration with high-magnification microscopy. Overall, this radial design and approach offer a novel solution for dynamic organ-on-a-chip cultures, utilizing standard laboratory tools for easy assembly, minimal

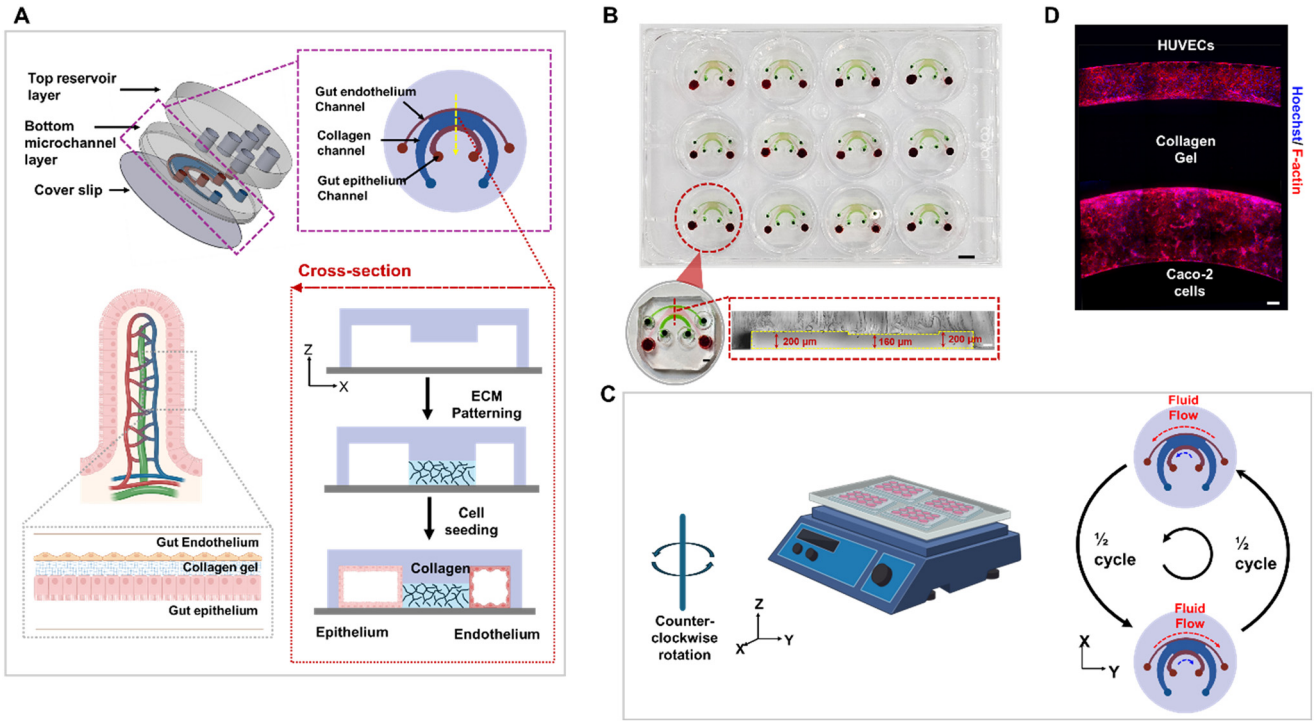

Fig. 1 Orbital shaker-driven radial microfluidic chip. (A) Schematic of the chip assembly. The glass coverslip, bottom PDMS layer (microchannel), and top PDMS layer (reservoir) are plasma bonded to complete the chip. The cross section of the microchannel shows the variable microchannel height to generate the CBV. Hydrogel is compartmentalized precisely in the shallower (center) channel and the taller channels on either side serve to culture gut epithelium and gut endothelium. The overall gut-on-a-chip replicates a section of the intestinal villi–gut vasculature axis. (B) The microfluidic chips inside the wells of a 12-well plate for parallelized operation (scale bar: 5 mm). The inset shows a magnified view of a chip (scale bar: 2 mm) and a cross-sectional view of a PDMS microchannel with variable channel heights (scale bar: 100 μm). (C) Orbital shaker-driven fluid stimulation results in a bidirectional flow. Multiple 12-well plates with chips can be mounted on an orbital shaker for flow actuation for a high-throughput operation. (D) Fluorescence large image of the chip showcasing the vasculature (HUVECs) and gut epithelium (Caco-2 cells) separated by collagen gel. Scale bar: 100 μm.

training, and seamless integration with detection modalities such as microscopy.

Orbital shaker-driven fluid flow characterization

To understand the fluid flow through the cell culture channels, computational fluid dynamics (CFD) simulations were performed, revealing variations in shear stress and velocity over one cycle of the shaker operating at 100 rpm. The chip completes one cycle in 0.6 s around the axis of the shaker. The time-averaged shear stress and velocity over one cycle in the outer channel (gut endothelium) were 0.44 dyne cm^{-2} and 0.124 mm s^{-1}, respectively, and that for the Caco-2 channel were 0.32 dyne cm^{-2} and 0.091 mm s^{-1}, respectively (Fig. 2B and C). The higher shear stress and velocity in the gut endothelium can be attributed to its lower cross-sectional dimensions ($w \times h$ = 400 μm × 200 μm) as compared to the epithelial channel ($w \times h$ = 600 μm × 200 μm). It is noteworthy that the direction of flow in the two channels is opposite to that of the direction of rotation of the shaker. CFD simulation showcased the bidirectional flow, with a temporal net flow in the clockwise direction when the shaker is set to counterclockwise rotation. Experimental flow characterization using 1 μm beads proved the presence of flow opposite to the direction of rotation of the orbital shaker (Fig. S2). These results indicate inertial flow within the channels with the particles experiencing forces opposite to the direction of rotation. As expected, simulations revealed that the magnitude of time-averaged shear stress and velocity are directly proportional to the rotational speed of the shaker (Fig. S3). By adjusting the orbital shaker from 50 rpm to 200 rpm, the time-averaged shear stress can be increased from 0.17 dyne cm^{-2} to 1.74 dyne cm^{-2} in the gut endothelium channel and from 0.12 dyne cm^{-2} to 1.34 dyne cm^{-2} for the gut epithelium channel (Fig. S3D). The time-averaged velocity followed a similar trend, varying from 0.0521 mm s^{-1} to 0.28 mm s^{-1} for gut endothelium and 0.0410 mm s^{-1} to 0.25 mm s^{-1} for gut epithelium (Fig. S3H). These differences in shear stress and velocity between the two channels were a function of cross-sectional area with negligible impact of the radii of curvature (gut endothelium *vs.* gut epithelium = 8 mm *vs.* 3.8 mm) or length of the channels.

Fluid simulations also highlighted the temporal fluctuations to fluid shear stress and velocity over the duration of one orbital cycle. At 100 rpm, shear stress and velocity cycled from high (0.73 dyne cm^{-2} and 3.4 mm s^{-1}) to low (0.24 dyne cm^{-2} and 0 mm s^{-1}) and then back to high (Fig. 2D and E). Interestingly, the vector plot of fluid

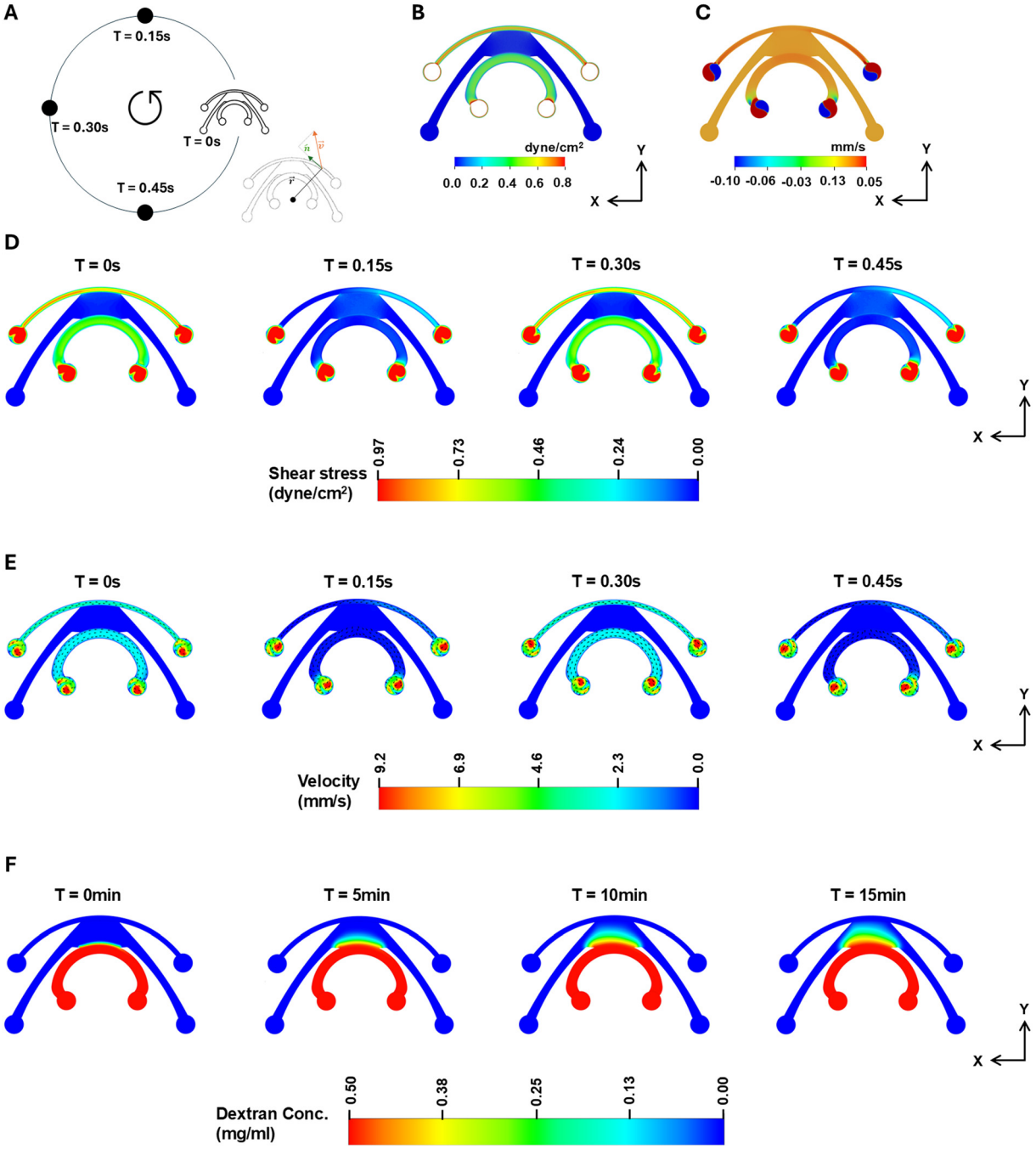

Fig. 2 Computational fluid dynamics simulations. (A) Scheme highlighting the radial position of the chip during one cycle on the orbital shaker (counterclockwise rotation at 100 rpm). (B) Time-averaged shear stress in the outer and inner channels. (C) Time-averaged velocity in the outer and inner channels. (D) Shear stress simulations at different time points of one cycle. (E) Velocity vector and magnitude at different time points in one cycle. (F) Dextran diffusion through the collagen gel over 15 min showcasing the ability to study molecule diffusion using the platform. Dextran diffusion covers ~100% of the collagen gel between the inner and the outer channels within 15 min.

velocity revealed time-dependent changes in flow direction depending on the chip's orbital position every 0.3 s. For a counterclockwise orbital rotation, the fluid flow shifted from an initial clockwise direction to counterclockwise at the midpoint of the cycle (T = 0.3 s for 100 rpm), then fluctuated back to the initial clockwise direction by the end of the cycle. Apart from the cell culture channels, the chip houses the ECM, where the shear stress and velocity are negligible due to the porosity of the collagen gel. These mechanical properties of collagen make it an excellent medium for promoting the diffusion of molecules. CFD simulations of dextran diffusion under orbital stimulation demonstrated the potential of the collagen gel in generating a time-dependent gradient generation (Fig. 2F).

It is noteworthy that dextran diffusion under static conditions was negligible (Fig. S4), underlining the importance of the orbital forces in promoting the diffusion of dextran across the porous ECM. Overall, the flow profile generated under orbital stimulation is a bidirectional peristaltic (stop and go) flow in the gut epithelium and endothelium channels while promoting molecule diffusion across the ECM. The flow mechanism shares similarities to the mixing and shearing from the cyclic peristaltic mechanics of the human gut.[31,32]

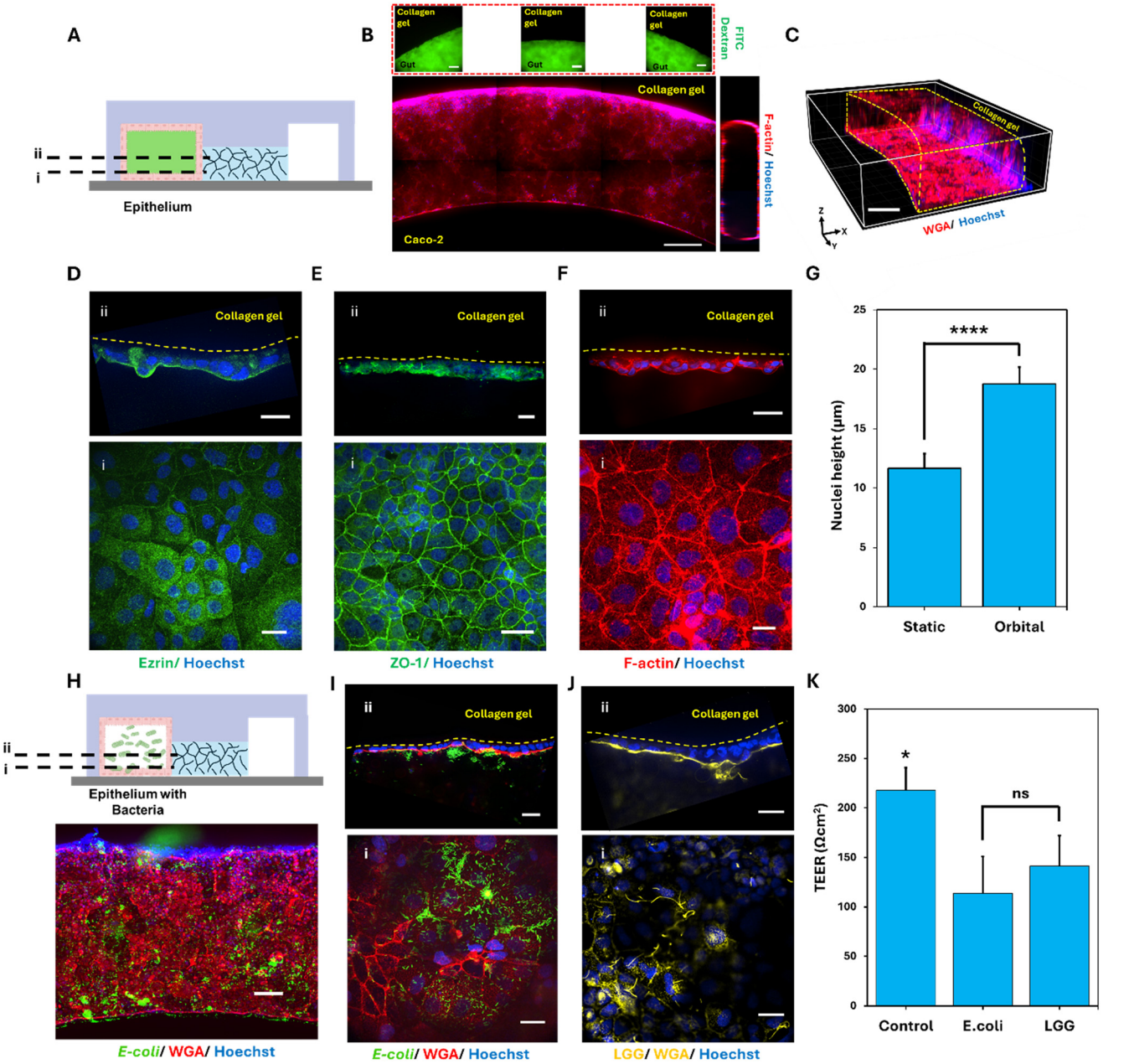

Fig. 3 Characterization of the biomimetic gut epithelial tube. (A) Cross-sectional schematic showing the gut epithelium tube and the collagen gel. Image labels i and ii refer to the different cross-sectional heights within the chip. (B) Fluorescence image of the gut tube after 5 days of orbital perfusion. Top inset highlights the intact gut tube filled with 40 kDa FITC-conjugated dextran. Right inset is the orthogonal view of the gut tube from confocal imaging signifying the culture of Caco-2 cells along the walls. Scale bar: 200 μm. (C) Isometric 3D image of the gut tube. Scale bar: 100 μm. High-magnification confocal image of (D) ezrin at the base of the chip and along the collagen gel (top). Caco-2 polarization is evident from ezrin expression in the apical side with limited expression on the basal side of the epithelium. Scale bar: 30 μm. (E) ZO-1 expression of Caco-2 cells at the base and along the collagen wall (top). Scale bar: 30 μm. (F) F-actin signifying the presence of microvilli on each cell. Intact F-actin expression is observed along the collagen gel (top). Scale bar: 30 μm. (G) An increase in nuclei height is observed for cells cultured under perfusion conditions. $N = 9$; $^{****}p < 0.00001$. (H) Host–microbiome interactions. Scheme showing the gut tube with bacteria. (Bottom) Large image of the gut tube highlighting GFP *E. coli* microcolonies after 24 h in culture. Image labels i and ii refer to the different cross-sectional heights within the chip. Scale bar: 100 μm. High-magnification images of (I) *E. coli* and (J) LGG at the base and on the cells along the collagen gel. Scale bar: 30 μm. (K) TEER measurements of gut barrier integrity after 24 h of bacterial incubation. $N = 3$; $^{*}p < 0.05$.

Orbital perfusion-driven gut-vasculature model

Human intestinal colorectal adenocarcinoma cells (Caco-2) were used to recapitulate the gut epithelium. Cells were seeded to ensure initial adhesion across all the walls of the gut epithelium channel, including the exposed surface of the collagen gel, and cultured for 4 days under the perfusion culture from orbital actuation. Leakiness of 40 kDa FITC conjugated dextran into the collagen gel was assessed to evaluate the gut barrier integrity (Fig. 3A and B). Confocal imaging revealed the formation of a confluent gut tube along the walls of the channel (Fig. 3B and C). The Caco-2 monolayer expressed key physiological traits of the gut such as cell polarization as evidenced by ezrin on its apical surface (Fig. 3D), tight junctions (zonula occludens-1, ZO-1; Fig. 3E), and microvilli on individual cells (Fig. 3F). An increase in the nuclei height of the Caco-2 cells was observed under orbital actuation in comparison to static culture (~19 μm *vs.* 12 μm), further indicating cell polarization (Fig. 3G and S5A and B). Besides microscopy, the chip design allows for other modalities of assessment such as transepithelial electrical resistance (TEER), an alternate indicator of monolayer integrity. TEER measurements of the Caco-2 monolayer across the collagen gel indicated the formation of a tighter gut epithelium under perfusion culture (280 Ω cm^2 *vs.* 148 Ω cm^2; Fig. S5C). To increase complexity and recreate a microbiota-residing gut microenvironment, we cultured gut bacteria in the intact gut tube. *E. coli* and *Lactobacillus rhamnosus* GG (LGG) were cultured for 24 h and microcolony formation was observed along the different walls of the gut epithelial tube (Fig. 3I and J and S5D). For visualization, all the cells were stained with Hoechst for their nuclei, and Caco-2 cells and LGG were stained with wheat germ agglutinin (WGA) that stained both mucin layers on the monolayer and the peptidoglycan of Gram-positive LGG, while *E. coli* expressed green fluorescent protein (GFP). Although prior studies[8] suggests the production of mucus from Caco-2 cells during dynamic culture, we added mucin exogenously into the cell culture medium to support bacterial attachment to the cell monolayer and facilitate their growth. Bacterial growth was not observed in the collagen gel, highlighting that bacteria cultured over 24 h did not breach the epithelium. Nevertheless, TEER measurements showed a drop in barrier resistance due to the presence of bacteria (114 ± 37 Ω cm^2 for *E. coli* and 142 ± 30 Ω cm^2 for LGG; Fig. 3K). Notably these measurements were comparable to TEER measurements for an intact gut tube cultured under static conditions (Fig. S5C). Overall, perfusion culture driven by orbital shaker facilitates the formation of an intact and polarized gut epithelial tube that supports effective bacterial colonization and confinement within the gut.

In addition to the gut epithelium, we replicated a gut endothelium using human umbilical vein endothelial cells (HUVECs) along the walls of the gut endothelium channel

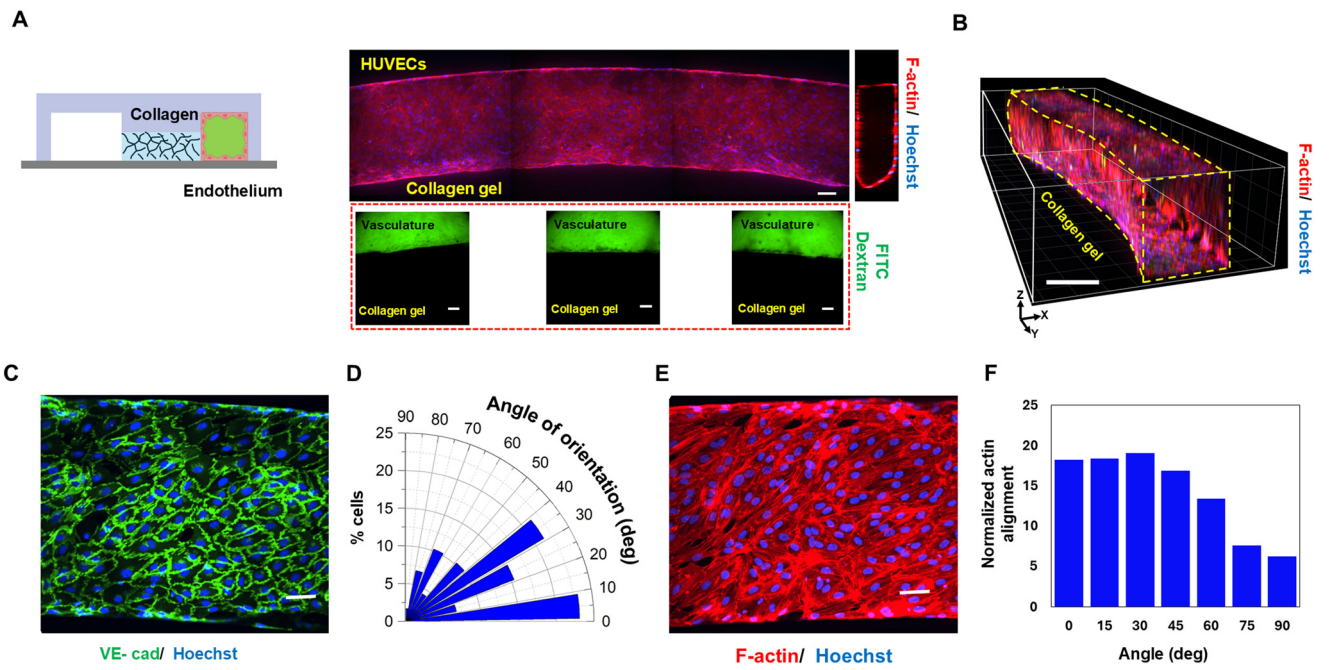

Fig. 4 Characterization of the biomimetic endothelial tube. (A) Cross-sectional schematic showing the endothelium tube. Fluorescence image of the endothelial tube. (Bottom) Inset shows the intact vasculature tube filled with 40 kDa FITC conjugated dextran. (Right) Inset showcases the orthogonal view of the endothelium tube signifying the culture of HUVECs along the channel walls. Scale bar: 200 μm. (B) Isometric 3D view of the vasculature tube. Scale bar: 100 μm. (C) Aligned HUVECs stained using VE-cadherin. Scale bar: 100 μm. (D) Radial plot highlighting a significant percentage (72%) of cells aligned in the direction of flow (<45°). (E) F-actin fibres in HUVECs. Scale bar: 100 μm. (F) Histogram signifying high percentage of alignment of the actin filaments (72%) in the direction of flow. The VE-cadherin cell alignment and actin alignment plot were calculated from 80 to 100 cells.

including the exposed surface of the collagen gel (Fig. 4A). After 4 days of orbital shaker-driven culture, HUVECs lined the walls, forming an intact vascular tube, which was confirmed using the dextran diffusion assay (Fig. 4A and B). The intact HUVEC monolayer was further characterized by continuous VE-cadherin expression (Fig. 4C), as confirmed by immunofluorescence staining. A key physiological trait of the blood vessels is alignment of endothelial cells along the direction of blood flow. In our platform, perfusion culture promoted the alignment of endothelial cells in the direction of flow. Quantification of VE-cadherin-based cell alignment showed a significantly high percentage of cells aligning in the direction of flow (0° to 45°) under perfusion culture compared to static culture (72% *vs.* 53%) (Fig. 4D and S6A). The bidirectional flow also resulted in the alignment (0° to 45°) of intracellular actin fibers (72% for perfusion *vs.* 53% for static) (Fig. 4E and F and S6B). However, unlike the gut epithelium, perfusion culture did not improve the integrity of the endothelial tight junctions (Fig. S6C). We have successfully created a physiologically relevant endothelial tube with the cells aligned parallel to the direction of flow. Notably, the gut epithelial and endothelial tubes are interconnected through the porous collagen gel, which facilitates paracrine signaling and paracellular absorption of molecules from gut. Furthermore, the ability to culture a biomimetic gut-vasculature model using orbital shaker-driven perfusion validates the benign nature of the bidirectional flow generated here and the potential of employing this simple tool to create multi-organ platforms with mechanically responsive cells.

Chemokine- or drug-induced permeability assay

Leakiness of epithelium and endothelium is a hallmark of a dysfunctional human gut. Previously, pro-inflammatory cytokines or drugs have been shown to disrupt the barrier function of the gut.[28,29,33] To study the potential for inducing leakiness in the endothelium and epithelium, we used tumor necrosis factor-α (TNF-α) and aspirin overdose, respectively. Tube permeability was measured using the fluorescence-based dextran diffusion method and TEER. No diffusion of 40 kDa dextran diffusion was observed from the endothelial tube under orbital perfusion over 8 h. However, treatment of the HUVEC tube with TNF-α resulted in a significantly increased vascular leakiness (Fig. 5A). A time-dependent increase in vascular leakiness was observed from TEER measurements. A significantly higher permeability was detected within 4 h of TEER measurements as opposed to 6 h

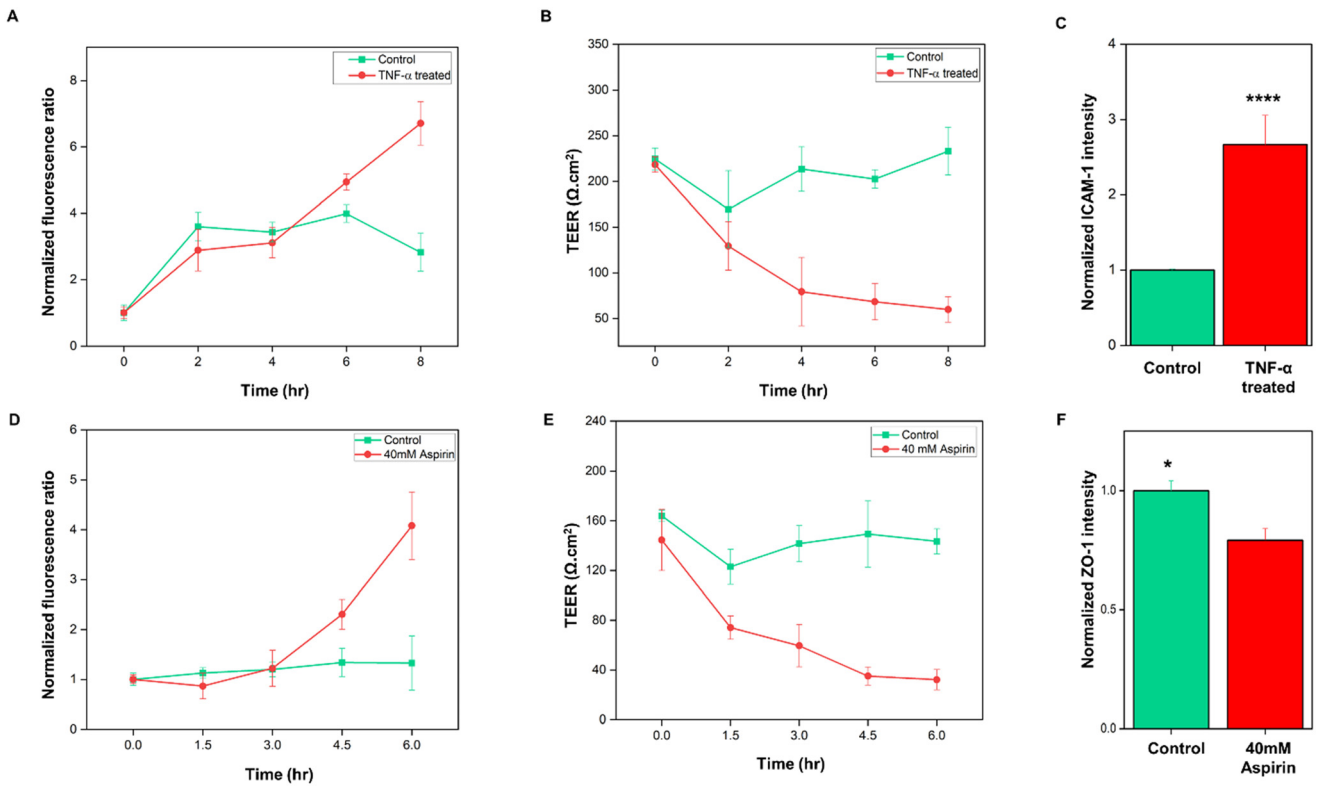

Fig. 5 Influence of drug or chemokine treatment on vasculature and gut epithelium. (A) Dextran permeability assay with and without TNF-α treatment on the endothelial tube indicates an increased permeability after 6 h of TNF-α treatment. $N = 3$. (B) TEER measurements corroborate the loss in endothelial barrier integrity over time upon TNF-α treatment. $N = 4$. (C) ICAM-1 expression is significantly upregulated after 8 h of TNF-α treatment. $N = 10$; ****$p < 0.00001$. (D) Dextran permeability assay highlighting the impact of high-dosage drug treatment on gut barrier integrity after 4.5 h. $N = 8$. (E) TEER measurements corroborate the loss in gut epithelial integrity over time. $N = 5$. (F) High dosage of aspirin impacts ZO-1 expression of gut epithelium after 6 h of treatment. $N = 6$; *$p < 0.05$.

during the fluorescence-based detection, highlighting the greater sensitivity of the TEER method (Fig. 5B). This increase in leakiness was attributed to the endothelial inflammation caused by the treatment with TNF-α. This was evident from the upregulation of intercellular adhesion molecule-1 (ICAM-1), a known indicator of inflammation expressed on the surface of endothelial cells (Fig. 5C).

To investigate gut permeability, we simulated the condition of a drug overdose by treating the gut tube with 40 mM aspirin. A high dosage of aspirin was treated on the Caco-2 tube for over 6 h. Dextran permeability for the untreated control was steady while an increase in gut leakiness was evident from the 4.5-h time point upon aspirin treatment (Fig. 5D). The dextran permeability assay corroborated TEER measurements in the gut tube treated with and without aspirin (Fig. 5E), with TEER detecting significantly high permeability after 1.5 h of aspirin treatment. As expected, aspirin overdosage reduced the expression of tight junction protein ZO-1 (Fig. 5F) compared to the untreated control. These investigations reaffirm the impact of high drug dosages on gut barrier integrity and inflammatory cytokines on vascular permeability. Furthermore, these studies validate our platform's utility for drug testing applications and its ability to support multimodal permeability studies, which is a key read-out for drug development.

Nanoplastic transfusion into vasculature

We explored the use of the gut-vasculature model to study nanoplastic absorption in an impaired gut. Fluorescent polyethylene terephthalate (PET) nanoparticles (100 nm and 200 nm) were introduced at a concentration of 1 mg ml^{-1} into the gut epithelium, and their absorption was evaluated in both intact and disrupted gut-vasculature systems. Drug-induced disruption of the gut and endothelium resulted in a visible increase in nanoplastic transfer from the gut tube through the collagen gel and into the vasculature (Fig. 6B and C). Briefly, we treated the gut tube with a high dose of aspirin and the endothelial tube with TNF-α to create an impaired gut-vasculature model. A scan across different chip sections highlighted a time-dependent increase in 100 nm particles from the gut epithelium through the collagen gel and into the vasculature over 18 h under orbital perfusion (Fig. 6D). Notably, the particles cross the impaired gut barrier to enter the collagen gel within 6 h of drug treatment. However, this was not observed in an untreated gut (Fig. S7). Interestingly, the gut barrier allowed a paracellular transfer of particles in a size-dependent manner. This was evident in the 200 nm particle studies where particles failed to cross over to the vasculature (Fig. 6E). These results mirror the issue of nanoplastic ingestion and its potential transfer into the bloodstream. While the barrier function of a healthy gut

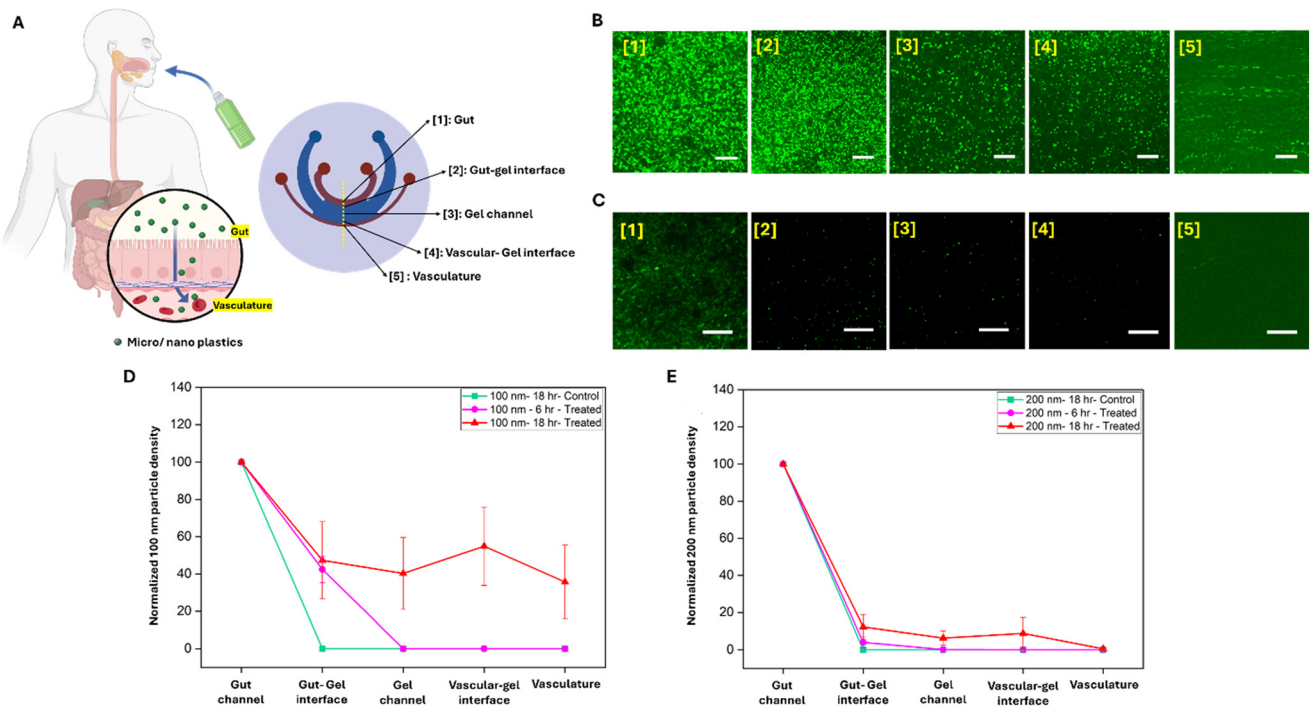

Fig. 6 (A) Nanoplastic poisoning is a consequential impact of impaired gut leading to particle entry into the systemic circulation. In our platform, 5 different points in the chip were assessed to quantify nanoplastic transfusion. High-magnification confocal images of (B) 100 nm and (C) 200 nm nanoplastic aggregates across the different positions within the chip. Scale bar: 20 μm. Nanoplastic density quantified from the fluorescence images for (D) 100 nm and (E) 200 nm particles. Under untreated conditions (control), the gut barrier permeability inhibited the nanoparticles from crossing into the collagen gel. However, a leaky gut and inflamed endothelium resulted in increased particle accumulation at different positions in the gut and vasculature system. A size-dependent permeability was observed with a higher density of 100 nm plastics transfusing to the vasculature in comparison to the 200 nm particles. $N = 6$.

prevents the penetration of such foreign agents into the bloodstream, an impaired gut fails to protect the vasculature from nanoplastic entry. However, the impaired gut epithelium persists for over 18 h, serving as a protective barrier against larger particles (200 nm). These results also highlight the potential of using such a platform for studying size-dependent particle absorption by the gut into the systemic circulation.

Discussion

The field of organ-on-a-chip has progressed considerably due to innovations in microfabrication, materials science, and detection technologies. However, its broader application still faces numerous challenges, including complex setup procedures, sample variability, large operational footprint, limited throughput, and the need for specialized instrumentation. While the use of standardized cell lines and harmonized cell culture practices can help reduce sample heterogeneity, engineering solutions are necessary to minimize dependence on skilled personnel and specialized tools. In this work, we present a user-friendly microfluidic platform designed to replicate the biomimetic and heterogeneous cellular environments of human organs. The microfluidics are encapsulated in a single PDMS layer, simplifying device assembly *via* direct plasma bonding to a glass coverslip. This eliminates the need for the specialized alignment tools and bonding methods required by current models.[9,27,34,35] The glass coverslips provide excellent *in situ* high-magnification imaging, facilitating easy integration with microscopes. Moreover, the pumpless design simplifies chip setup by removing the necessity for syringe or pressure pumps and their associated tubing networks. The miniaturized radial design and its incorporation as an insertable chip in a 12-well plate offers operational versatility compared to pre-designed platforms.[26,28] Additionally, the use of multiple stacked 12-well plates on an orbital shaker enables the simultaneous operation of over 100 chips, enhancing scalability. In line with contemporary gut-on-a-chip platforms, we observed the formation of tight junctions and a monolayer with strong barrier integrity within 4–5 days of on-chip culture[28] unlike the traditional static Transwell assays where Caco-2 culture and differentiation takes up to 21 days. Alternate studies have also highlighted the ability to achieve a well-differentiated epithelium within 7 days of culture in an organ-chip[8] configuration, highlighting the ability of such platforms to minimize overall culture time to create effective *in vitro* models. Additionally, the 4-day perfusion culture was optimal to maintain two cell lines, Caco-2 cells and HUVECs, with distinct cell growth characteristics. However, the culture duration is tunable and dependent on the study under investigation.

Extracellular matrix (ECM) patterning is commonly used in microfluidic organs-on-chips to compartmentalize cell chambers without the use of polymeric membranes. Our barrier-free ECM patterning eliminates the need for micropillars[36] or phaseguides,[28] enabling the creation of curvilinear channels, which enhances cell–ECM interactions and simplifies microfabrication. Besides the chip design, the unique pumpless method employed here utilizes orbital shakers to generate a bidirectional peristaltic flow profile with physiologically relevant shear stress.[31]

Orbital shakers are a mainstay in several biological laboratories for mammalian cell and bacterial cell cultures.[37] However, its use in organ-on-a-chip operations has not been explored due to the linear designs of conventional organ-chip platforms, where orbital shaker-driven flow is erratic in linear microchannels. As a result, centrifugal, gravity-driven, and rocker-based pumpless systems are typically used for linear organ-chip devices. Notably, fluctuating shear stress and bidirectional flow observed in this study are uncharacteristic of syringe pump-driven perfusion. However, they are common *in vivo*, particularly in the gut and vasculatures, where mechanical stimuli such as peristalsis result in fluctuating and bidirectional flow.[31,32]

We validated our model by recreating a gut-vasculature model. Human gut epithelial cells and endothelial cells form polarized biomimetic tubes under orbital flow stimulation. The two monolayer tubes were separated by a porous ECM layer, mimicking the basement membrane *in vivo* that separates the vasculature and the gut epithelium. Unlike rocker-based or gravity-driven models, orbital motion induces a dynamic pressure gradient on either side of the collagen gel, facilitating the active bidirectional transfer of small molecules, chemokines and nanoparticles between the gut and the vasculature. This replicates *in vivo* forces such as peristalsis and segmentation of the gut that play a role in mixing and transferring intestinal metabolites and molecules from the gut lumen into the blood. The model thus enhances the relevance of studying nutrient absorption, the effects of prebiotics on gut health, and chemokine-induced gut dysbiosis.

The human intestine is a complex organ with numerous functions, making it challenging to replicate an all-encompassing gut using a single *in vitro* model. In our study, we have developed a platform to potentially study host–microbiome interactions, drug testing, and the consequences of an impaired gut. As a proof of concept, we demonstrated bacterial colonization using *E. coli* and LGG within the gut epithelium. We also tested the effects of known endothelial and gut epithelial disruptors to validate drug-induced permeability assays. These applications were facilitated by the ability to perform high-magnification and high-resolution imaging, and TEER measurements owing to the compartmentalized design. TEER measurements are influenced by multiple factors including cell type, passage number, cell culture medium, culture conditions such as the presence of unidirectional fluid flow, culture duration, and the methodology and tools used for measurement. Interestingly, the TEER values observed in our study for Caco-2 culture differs from the Caco-2 culture in traditional Transwell assay.[9] These differences between the two models can be attributed to several factors, including variations in

dimensions, cell culture medium resistance, culture duration, non-uniform current density across the monolayer, electrode positioning, and the use of different TEER measurement tools during measurement. Nonetheless, our measurements are consistent with several contemporary organ-on-a-chip models,[26,38] with comparable dimensions, cell types, cell passage numbers and shear profiles. It is noteworthy that TEER values vary across gut-on-a-chip platforms. For example, TEER measurements of our platform with a monolayer tube of Caco-2 cells were lower in comparison to the continuous flow-based platforms developed by Kim *et al.*,[9] where the unidirectional flow of cell culture medium over 7 days of culture resulted in multi-layered Caco-2 culture with significantly higher cell density, which increases the resistance across the monolayer. Nonetheless, our membrane-free, pumpless, 4-day monolayer tube showcased functional gut barrier integrity, which was further evident from the dextran diffusion studies. Taken together, this model serves as a valuable tool for testing and novel therapeutic development, particularly for exploring bacteria-induced drug responses.[39]

Microplastic pollution is a global health crisis caused by the infiltration of particles smaller than 5 mm into the human body through food, water and air.[40] These particles infiltrate the systemic circulation *via* intestinal absorption triggering systemic inflammation, gut dysbiosis, cardiovascular disorders, and autoimmune diseases.[41,42] Nanoplastics are a subtype of microplastics that are less than 1 μm in size. Our gut-vasculature model reveals how healthy gut health alleviated nanoplastic penetration through the gut epithelium. In contrast, we observed a heightened cross-over of particles across the gut triggered by drug-induced gut impairment. While animal and organoid models have been used to study particle infiltration,[43] our platform generates relevant biomechanical cues that offer unique insights and visual evidence of the passage of particles through a disrupted epithelium and into an inflamed vasculature in a biomimetic microenvironment. In addition to providing insight into pathways of foreign agent entry, this platform can potentially be used to test therapeutic interventions, such as microbiome modulation or prebiotics, to minimize micro-/nanoplastic poisoning.

It is noteworthy that the low flow rates using this approach make it unsuitable for developing organ-chips requiring atherogenic or turbulent flow profiles.[44] The lack of continuous fluid clearance such as that provided by syringe or pressure pump-driven perfusion[8,45] limits long-term bacterial culture studies. These drawbacks reduce its potential for studying pathologies such as atherosclerosis and microbial ecology in the gut. Caco-2 cells and HUVECs used in the study are commonly used to recapitulate *in vitro* gut epithelium and endothelium, respectively. The use of these cell lines ensured high reproducibility and direct comparison with existing literature, both of which are necessary for effective validation of a new methodology. In future studies we intend to use targeted-application-specific primary intestinal epithelial cells, microvasculature and immune cells to enhance their physiological relevance and the ability to mimic immune-regulated gut processes.

Conclusion

In summary, we have designed a simple yet effective organ-on-a-chip and developed a novel approach for operating these chips using a standard orbital shaker. This innovation simplifies chip assembly, eliminates the need for complex instrumentation, and hence, democratizes access to organ-on-a-chip technology. The platform supports multimodal detection, including high-magnification microscopy and alternative modalities such as TEER, enhancing its user-friendliness and the potential for miniaturization of the set-up. The successful creation of gut epithelial and endothelial monolayer tubes enables studies of drug-induced permeability and particle transfusion across the leaky gut. This scalable, biomimetic platform holds great promise for studying pathophysiology, drug development, and immune-regulated, microbe-colonized gut-on-a-chip models. Furthermore, it offers unique opportunities to investigate gut-related diseases, including inflammatory conditions, drug absorption, and micro-/nanoplastic-induced health concerns, making it a powerful tool for advancing biomedical research and therapeutic development.

Methods

Fabrication of radial microfluidic chips

The chip comprises two layers of PDMS created using soft lithography: the bottom microfluidic layer with the channels and a top reservoir layer. The mold for the microfluidic channels was fabricated by SU-8 photolithography on a silicon wafer, which was subsequently silanized with trichloro(1*H*,1*H*,2*H*,2*H*-perfluorooctyl)silane (Sigma Aldrich). The mold of the reservoir layer was 3D printed using a benchtop 3D printer (Formlabs). Both layers were fabricated by mixing elastomer and curing agent (SYLGARD™ 184) of weight ratio 10 : 1, followed by degassing and curing at 70 °C for 24 h. After fabrication, each layer was cleaned using IPA through sonication (Sono Swiss) for 15 min. The bottom layer was initially bonded to the glass coverslip *via* oxygen plasma treatment (Tergeo, Pie Scientific LLC) and cured at 70 °C for 2 h. Subsequently, the top layer was then bonded to the upper surface of the bottom layer using the same procedure and the assembled chip was placed overnight at 70 °C.

Cell culture and establishing the monolayer tubes

The Caco-2 cell line was a kind gift from Professor Gigi N. C. Chiu from the Department of Pharmacy at the National University of Singapore. Caco-2 cells between passages 63 and 70 were maintained in EMEM (Lonza), supplemented with 20% FBS (Lonza) and 1% penicillin/streptomycin mix (Lonza), and were used in the experiment. Human umbilical vein endothelial cells (HUVECs; Cell Applications, Inc.)

between passages 4 and 8 were maintained using endothelial cell growth medium-2 (EGM-2) (BulletKit, Lonza) supplemented with 1% penicillin/streptomycin. All the cells were cultured to 80% confluency at 37 °C in a humidified 5% CO_2 incubator. Confluent layers were dissociated using TrypLE™ Express Enzyme (Gibco) and homogenized to a cell concentration of 1 million cells per ml for Caco-2 cells and 2 million cells per ml for HUVECs.

Prior to culturing cells inside the microfluidic chip, the chips are UV sterilized for 30 min. Subsequently, collagen (rat tail type I collagen) (Ibidi GmbH) at a concentration of 4 mg ml^{-1} was introduced to the central ECM channel and placed at 37 °C for thermal gelation. This compartmentalized the chip into three channels: the center ECM channel and the two side channels. A coating solution composed of 150 μg ml^{-1} Matrigel (Corning), 25 μg ml^{-1} bovine type I collagen (Ibidi GmbH) and 25 μg ml^{-1} fibronectin (Thermo Fisher) in serum-free EMEM is introduced into the side channels for 1.5 h. After washing the channel with serum-free medium, Caco-2 cells and HUVECs were introduced into the inner and outer channels of the radial chip. To ensure that the cells are seeded across all the walls of the channels, the chip was overturned and subsequently tilted from one side to the other and maintained at each position for 15 min. After cell seeding, 60 μl of the respective cell culture medium was introduced to the inlets and outlets of the channels and the chips are placed in a humidified incubator at 37 °C and 5% CO_2 overnight. Following this, the chips are transferred to a 12-well plate and placed on an orbital shaker that is set to operate at a speed of 100 rpm. The orbital shaker with the chips is placed inside the CO_2 incubator (37 °C and 5% CO_2) for 4 days to form the confluent monolayer tubes of gut epithelium and endothelium.

Monolayer permeability

One method to measure the permeability of the gut epithelial tube and endothelial tube was using FITC-conjugated 40 kDa dextran (Sigma). For healthy epithelium and endothelium, dextran at a concentration of 0.5 mg ml^{-1} in the specific cell culture medium was introduced into the respective channels. Fluorescence images were acquired over 8 h at 2 h intervals for the endothelial tube and over a period of 6 h at intervals of 1.5 h. To induce leakiness, the dextran medium for the gut tube was supplemented with 40 mM acetylsalicylic acid (aspirin; Sigma), and the medium for the endothelial tube was supplemented with10 ng ml^{-1} TNF-α (Thermo Fisher). Images were recorded for the duration and intervals specified for the healthy control experiments. To calculate leakiness, the ratio of the fluorescence intensity inside the collagen gel and the intensity inside the channel were calculated and normalized to the measurements at time 0 min. All experiments were replicated at least three times.

Alternatively, TEER measurements also enabled the quantification of barrier integrity. TEER was measured using a 2-wire resistance method with Keithley DMM6500 6.5 Digit Multimeter (Tektronix). Two copper wires were inserted into the chips' outlets to measure the current across two cell channels (Fig. S8). Briefly, for epithelial monolayer resistance, Caco-2 cells (and no HUVECs) were cultured to a monolayer tube for 4 days under orbital actuation in the respective channel, followed by measuring the electrical resistance of the Caco-2–gel interface as shown in Fig. S8. Similarly, endothelial monolayer electrical resistance was measured from a chip with only the HUVECs tube. Data were recorded after 30 seconds to allow for stabilization of the readings. Resistance from blank chips containing only a collagen matrix and medium without cells was also recorded to correct cell monolayer resistance measurements and negate the effects of material properties (ECM, medium) on the resistance values. At least three independent chips were measured for each TEER condition.

Immunofluorescence staining

To perform on-chip immunofluorescence staining, the cells within the channels were first fixed with 4% paraformaldehyde (PFA) for 10 min to preserve their morphology. Subsequently, the cells were permeabilized using 0.2% Triton X-100 for 15 min to facilitate antibody penetration. The sample was then blocked with 1% bovine serum albumin (BSA) for 2 h to reduce non-specific binding. Following this, the Caco-2 cells was incubated overnight at 4 °C with primary antibodies targeting specific Caco-2 cells, including anti-ZO-1 (Invitrogen, 61-7300) and anti-Villin1[R814] (Cell Signaling Technology, 2369) for staining ezrin and HUVECs were stained using anti-CD31 for VE-cadherin (Abcam, ab24590). After washing, the sample was further incubated with a secondary antibody, goat anti-rabbit IgG H&L (Alexa Fluor 488), at room temperature for 1 h in the dark. Both Caco-2 cells and HUVECs were stained for their nucleus and actin filaments using Hoechst 33342 and Phalloidin-iFluor 647, respectively. HUVECs inflammation was monitored using PE-labelled anti-human CD54 (Biolegend) to detect intercellular adhesion molecule-1 (ICAM-1). For ICAM-1 staining, HUVECs treated for 8 h with or without TNF-α were stained for 30 min and imaged immediately, without cell fixation.

Bacteria culture on-chip and staining

Both GFP-tagged *E. coli* (ATCC 25922™) and *Lactobacillus rhamnosus* strain GG (LGG) (ATCC 53103) were obtained from ATCC. GFP *E. coli* was cultured on LB agar (Invitrogen), while LGG was grown on MRS agar (Oxoid) under aerobic conditions, following ATCC guidelines. After 24 h of cultivation, GFP *E. coli* and LGG were prepared at concentrations of 10^6 CFU ml^{-1} and 5×10^6 CFU ml^{-1} in antibiotic-free medium (EMEM + 20% FBS), respectively, for inoculation with the gut tube. Before introducing bacteria into the chip, the medium for the Caco-2 tube was replaced with antibiotic-free medium containing 75 μg ml^{-1} porcine mucin (Sigma-Aldrich M2378) for 24 h. This helps clear any

residual antibiotics inside the chip and also ensures the presence of mucin to assist in bacterial adhesion. *E. coli* at the desired concentration was introduced and inoculated for 1.5 h and LGG was inoculated for 2 h. Bacteria inoculation was performed under static conditions. After the inoculation step is completed, the gut tube was washed with the antibiotic-free medium containing mucin, and 60 μl of this medium was added to the gut tube channel and placed on the orbital shaker (rotational speed of 100 rpm). The bacteria were then cultured for 24 h. Bacterial staining was performed using the live bacterial Gram staining kit (Biotium, 32000) according to the manufacturer's protocol. The chips were washed with BSA–NaCl buffer (0.25% BSA, 0.15 M NaCl in PBS) and incubated with CF™594 wheat germ agglutinin (WGA) dye at room temperature for 15 min. After another wash with BSA–NaCl buffer, the chips were stained with Hoechst 33342 (Thermo Fisher Scientific) for 10 min, followed by additional washing with BSA–NaCl buffer and fixation with 4% paraformaldehyde.

Nanoplastic transfusion study

To investigate nanoplastic escape from the gut into the vasculature, the gut tube and endothelial tube were disrupted using 40 mM aspirin (for 6 h) and 10 ng ml^{-1} TNF-α (for 8 h), respectively. Following this, 100 nm and 200 nm PET fluorescent (FITC) particles (Zhongke Keyou) were introduced into the gut tube channel. Different sections of the chip were imaged after 18 h of orbital actuation and the FITC images were acquired to determine the density of the particles in different sections of the chip between the gut and the vasculature. At least 3 different experiments were conducted for data analysis.

Computational fluid dynamic simulation

The fluid simulation was conducted using ANSYS Fluent (version 2023 R2, ANSYS Inc., Canonsburg, PA, USA) on a workstation equipped with an Intel Core i7-13700 CPU, 64 GB of RAM, and an NVIDIA GeForce RTX A5000 GPU. Given the low Reynolds number of the fluid profile, the simulation was executed in a laminar regime. The mesh for the endothelial channel, collagen channel, and Caco2 channel consists of 454 426, 538 611, and 586 367 elements, respectively. The fluid dynamics follow the principles of mass and momentum conservation.

$$\nabla \cdot \boldsymbol{u} = 0 \tag{1}$$

$$\rho((\boldsymbol{u}\cdot\nabla)\boldsymbol{u}) = -\nabla p + \mu\nabla^2\boldsymbol{u} \tag{2}$$

where $\boldsymbol{u}$ and p represent the velocity and pressure. Gravity was removed due to the microscale of the system. Ambient pressure was applied at all outlets. The whole mesh was translated circularly to mimic the rotation of the orbital shaker. The time-dependent velocity profile of the mesh is:

$$u_x = -r\omega \sin(\omega t) \tag{3}$$

$$u_y = r\omega \cos(\omega t) \tag{4}$$

where r and ω represent the orbital radius (9.5 mm) and angular frequency (10.47 rad s^{-1}), respectively. The tangent velocity was calculated as the dot product of the velocity vector and the tangent unit vector ($\hat{n}$) at each point. The tangent vector was selected to be perpendicular to the radius vector ($\vec{r}$) and pointed counterclockwise following the direction of orbital translation. The culture media for both endothelial and Caco2 cells were modeled to exhibit water-like properties, featuring a 1000 kg m^{-3} density and a 0.001 Pa s viscosity. The collagen network was modeled to have a porosity of 0.67 (ref. 46) and permeability of 7.8729×10^{-11} m^{-2}.[47] The diffusion coefficient of 40 kDa dextran (5.4×10^{-11} m^2 s^{-1}) was calculated using the scaling law proposed by Gribbon and Hardingham.[48] The equations were solved using a coupled solver with a second-order discretization scheme, employing a time step of 0.005 seconds. All data were collected from the fourth translation cycle, as the system may need the initial cycles to stabilize the flow.

For flow visualization, 1 μm fluorescent beads (FluoSpheres™, Invitrogen) were introduced into the right outlet of the endothelial channel (without cells) and the orbital shaker was operated at 100 rpm in the clockwise direction. Images of the entire channel were recorded at different time intervals using a CMOS camera (Thor DCC1645C) mounted on a Leica MZ125 stereomicroscope to track the leading edge of the bead flow in the counterclockwise direction.

Morphological analysis

Imaging was conducted using spinning disk confocal microscopy comprising an inverted microscope (Ti-E, Nikon), a spinning disk scan head (CSU-W1; Yokogawa), an sCMOS camera (Prime95B; Teledyne Photometrics) and a laser system (iLaunch; GATACA Systems). The 3D image analysis was performed using IMARIS (Bitplane Scientific software). ImageJ was used to calculate HUVEC alignment from VE-cadherin and F-actin images, ICAM-1 intensity measurement, ZO-1 intensity quantification, dextran diffusion analysis and the nanoparticle density quantification.

Statistical analysis

All data were generated from a minimum of three repeated chips ($n = 3$). Unless otherwise noted, numerical data were presented as mean ± standard deviation (SD). The statistical significance between the two groups was determined using Student's t-test with $P < 0.05$ indicating a significant difference.

Author contributions

NVM, LJY and CTL initiated and formulated the study. NVM, LJY and CTL planned the experiments. NVM designed and optimized the microfluidic chip and its operation. LJY

optimized the assay. TDH conducted the CFD simulations and BS fabricated the microfluidic chips. NVM, LJY, TDH and BS conducted the experiments and data analysis. NVM, LJY and CTL drafted the manuscript.

Conflicts of interest

There are no conflicts to declare.

Data availability

Supplementary information is available. See DOI: **https://doi.org/10.1039/D5LC00333D**.

Additional figures and data such as timelapse of beads flow under orbital stimulation, CFD at different orbital shaker conditions, cell culture under static conditions and control experiments for nanoplastic transfusion are included in the SI.

Acknowledgements

The authors would like to acknowledge financial support by the Startup Grant (Grant no. A-8001301-00-00) and the Institute for Health Innovation and Technology Grant (Grant no. A-0001415-06-00) from the National University of Singapore (NUS) and the NUS Mechanobiology Institute Mid-Sized Grant (Grant no. A-8001978-04-00) from the National Research Foundation. We express our appreciation to Associate Professor Gigi N. C. Chiu for generously providing the Caco-2 cell line. Furthermore, we acknowledge and appreciate the support provided by the Nano and Microfabrication Core, Microscopy Core, and Wet Lab Core at Mechanobiology Institute, NUS.

References

1 X. Wang, Y. Zhu, Z. Cheng, C. Zhang, Y. Liao, B. Liu, D. Zhang, Z. Li and Y. Fang, *Acta Biomater.*, 2024, **188**, 48–64.
2 C. Xian, J. Zhang, S. Zhao and X.-G. Li, *J. Tissue Eng.*, 2023, **14**, 20417314221149882.
3 Y. Yamaura, B. D. Chapron, Z. Wang, J. Himmelfarb and K. E. Thummel, *Drug Metab. Dispos.*, 2016, **44**, 329–335.
4 C. W. Wright, N. Li, L. Shaffer, A. Hill, N. Boyer, S. E. Alves, S. Venkataraman, K. Biswas, L. A. Lieberman and S. Mohammadi, *Sci. Rep.*, 2023, **13**, 16357.
5 D. Dutta and H. Clevers, *Curr. Opin. Immunol.*, 2017, **48**, 15–22.
6 T. L. A. Nguyen, S. Vieira-Silva, A. Liston and J. Raes, *Dis. Models Mech.*, 2015, **8**, 1–16.
7 J. Walter, A. M. Armet, B. B. Finlay and F. Shanahan, *Cell*, 2020, **180**, 221–232.
8 J. Lee, N. V. Menon and C. T. Lim, *Adv. Sci.*, 2024, **11**, 2302113.
9 H. J. Kim, D. Huh, G. Hamilton and D. E. Ingber, *Lab Chip*, 2012, **12**, 2165–2174.
10 J. Lee, N. V. Menon, H. D. Truong and C. T. Lim, *Small*, 2025, **21**, 2410258.
11 S. Jalili-Firoozinezhad, F. S. Gazzaniga, E. L. Calamari, D. M. Camacho, C. W. Fadel, A. Bein, B. Swenor, B. Nestor, M. J. Cronce, A. Tovaglieri, O. Levy, K. E. Gregory, D. T. Breault, J. M. S. Cabral, D. L. Kasper, R. Novak and D. E. Ingber, *Nat. Biomed. Eng.*, 2019, **3**, 520–531.
12 M. Maurer, M. S. Gresnigt, A. Last, T. Wollny, F. Berlinghof, R. Pospich, Z. Cseresnyes, A. Medyukhina, K. Graf and M. Groeger, *Biomaterials*, 2019, **220**, 119396.
13 N. V. Menon, H. M. Tay, K. T. Pang, R. Dalan, S. C. Wong, X. Wang, K. H. H. Li and H. W. Hou, *APL Bioeng.*, 2018, **2**(1), 016103.
14 S. K. Srivastava, G. W. Foo, N. Aggarwal and M. W. Chang, *Biotechnol. Notes*, 2024, **5**, 8–12.
15 T. E. Winkler, M. Feil, E. F. G. J. Stronkman, I. Matthiesen and A. Herland, *Lab Chip*, 2020, **20**, 1212–1226.
16 K.-Y. Shim, D. Lee, J. Han, N.-T. Nguyen, S. Park and J. H. Sung, *Biomed. Microdevices*, 2017, **19**, 37.
17 S. Y. Lee, H. J. Byun, H. Choi, J.-I. Won, J. Han, S. Park, D. Kim and J. H. Sung, *Biotechnol. Bioprocess Eng.*, 2022, **27**, 221–233.
18 M. B. Esch, H. Ueno, D. R. Applegate and M. L. Shuler, *Lab Chip*, 2016, **16**, 2719–2729.
19 L. C. Delon, A. Nilghaz, E. Cheah, C. Prestidge and B. Thierry, *Adv. Healthcare Mater.*, 2020, **9**, 1901784.
20 S. Gunasekera, B. Thierry, E. Cheah, B. King, P. Monis, J. M. Carr, A. Chopra, M. Watson, M. O'Dea and U. Ryan, *bioRxiv*, 2024, preprint, DOI: **10.1101/2024.07.07.602413**.
21 Y. Wang, Z. Shao, W. Zheng, Y. Xie, G. Luo, M. Ding and Q. Liang, *Biofabrication*, 2019, **11**, 045001.
22 Y. Guo, Y. Xie and J. Qin, *Biotechnol. J.*, 2024, **19**, 2300390.
23 M. Busek, A. Aizenshtadt, T. Koch, A. Frank, L. Delon, M. A. Martinez, A. Golovin, C. Dumas, J. Stokowiec and S. Gruenzner, *Lab Chip*, 2023, **23**, 591–608.
24 K. N. Kaiser, J. R. Snyder, R. A. Koppes and A. N. Koppes, *Adv. Funct. Mater.*, 2024, **34**, 2409718.
25 T. Ching, A. C. I. van Steen, D. Gray-Scherr, J. L. Teo, A. Vasan, J. Jeon, J. Shah, A. Patel, A. E. Stoddard, J. L. Bays, J. Eyckmans and C. S. Chen, *Lab Chip*, 2025, **25**, 1474–1488.
26 M. Morelli, M. Cabezuelo Rodríguez and K. Queiroz, *Sci. Rep.*, 2024, **14**, 5797.
27 P. Shah, J. V. Fritz, E. Glaab, M. S. Desai, K. Greenhalgh, A. Frachet, M. Niegowska, M. Estes, C. Jäger, C. Seguin-Devaux, F. Zenhausern and P. Wilmes, *Nat. Commun.*, 2016, **7**, 11535.
28 S. J. Trietsch, E. Naumovska, D. Kurek, M. C. Setyawati, M. K. Vormann, K. J. Wilschut, H. L. Lanz, A. Nicolas, C. P. Ng, J. Joore, S. Kustermann, A. Roth, T. Hankemeier, A. Moisan and P. Vulto, *Nat. Commun.*, 2017, **8**, 262.
29 N. V. Menon, H. M. Tay, S. N. Wee, K. H. H. Li and H. W. Hou, *Lab Chip*, 2017, **17**, 2960–2968.
30 C. Su, N. V. Menon, X. Xu, Y. R. Teo, H. Cao, R. Dalan, C. Y. Tay and H. W. Hou, *Lab Chip*, 2021, **21**, 2359–2371.
31 P. W. M. Janssen, R. G. Lentle, P. Asvarujanon, P. Chambers, K. J. Stafford and Y. Hemar, *J. Physiol.*, 2007, **582**, 1239–1248.
32 M. Boland, *J. Sci. Food Agric.*, 2016, **96**, 2275–2283.
33 C. Beaurivage, A. Kanapeckaite, C. Loomans, K. S. Erdmann, J. Stallen and R. A. J. Janssen, *Sci. Rep.*, 2020, **10**, 21475.
34 S. Hosic, A. J. Bindas, M. L. Puzan, W. Lake, J. R. Soucy, F. Zhou, R. A. Koppes, D. T. Breault, S. K. Murthy and A. N. Koppes, *ACS Biomater. Sci. Eng.*, 2021, **7**, 2949–2963.

35 O. T. P. Nguyen, P. M. Misun, A. Hierlemann and C. Lohasz, *Adv. Healthcare Mater.*, 2024, **13**, 2302454.
36 S. Chung, R. Sudo, P. J. Mack, C.-R. Wan, V. Vickerman and R. D. Kamm, *Lab Chip*, 2009, **9**, 269–275.
37 F. Meng, H. Cheng, J. Qian, X. Dai, Y. Huang and Y. Fan, *Med. Nov. Technol. Devices*, 2022, **15**, 100143.
38 M. Lucchetti, K. O. Aina, L. Grandmougin, C. Jäger, P. Pérez Escriva, E. Letellier, A. S. Mosig and P. Wilmes, *Adv. Healthcare Mater.*, 2024, 2303943.
39 M. Yadav and N. S. Chauhan, *Gastroenterol. Rep.*, 2021, **10**, 1–19.
40 S. S. Bora, R. Gogoi, M. R. Sharma, Anshu, M. P. Borah, P. Deka, J. Bora, R. S. Naorem, J. Das and A. B. Teli, *Front. Cell. Infect. Microbiol.*, 2024, **14**, 1492759.
41 N. Chartres, C. B. Cooper, G. Bland, K. E. Pelch, S. A. Gandhi, A. BakenRa and T. J. Woodruff, *Environ. Sci. Technol.*, 2024, **58**, 22843–22864.
42 C. E. Sofield, R. S. Anderton and A. M. Gorecki, *Curr. Issues Mol. Biol.*, 2024, **46**, 4186–4202.
43 S. B. Park, W. H. Jung, K. J. Choi, B. Koh and K. Y. Kim, *Tissue Eng. Regener. Med.*, 2023, **20**, 49–58.
44 N. V. Menon, C. Su, K. T. Pang, Z. J. Phua, H. M. Tay, R. Dalan, X. Wang, K. H. H. Li and H. W. Hou, *Biofabrication*, 2020, **12**, 045009.
45 A. Grassart, V. Malardé, S. Gobaa, A. Sartori-Rupp, J. Kerns, K. Karalis, B. Marteyn, P. Sansonetti and N. Sauvonnet, *Cell Host Microbe*, 2019, **26**, 435–444, e434.
46 V. Olivares, M. Cóndor, C. Del Amo, J. Asín, C. Borau and J. M. García-Aznar, *Microsc. Microanal.*, 2019, **25**, 971–981.
47 V. Serpooshan, M. Julien, O. Nguyen, H. Wang, A. Li, N. Muja, J. E. Henderson and S. N. Nazhat, *Acta Biomater.*, 2010, **6**, 3978–3987.
48 P. Gribbon and T. E. Hardingham, *Biophys. J.*, 1998, **75**, 1032–1039.

